processes

MDPI

Article

Effects of Heterogeneous Sulfated Acid Photocatalysts and Irradiation of Ultraviolet Light on the Chemical Conversion and Characteristics of Antifreeze from Bioglycerol

Cherng-Yuan Lin * and Yun-Chih Chen

Department of Marine Engineering, National Taiwan Ocean University, Keelung 20224, Taiwan; cyzclare@gmail.com

* Correspondence: lin7108@ntou.edu.tw; Tel.: +886-2-24622307

Abstract: The purity of crude glycerol, a by-product of biodiesel production, may be as low as 50%. Thus, it has relatively low economic value without previously applying adequate physical purification or chemical conversion processes. A solid-state sulfated acid photocatalyst, TiO_2/SO_4^{2-} was prepared in this study to catalyze the chemical conversion of bioglycerol with acetic acid to produce an antifreeze of glycerine acetate to improve the low-temperature fluidity of liquid fuel. The experimental results show that similar X-ray intensity structures appeared between the catalysts of TiO_2/SO_4^{2-} and SO_4^{2-}. An infrared spectra analysis using a Fourier transform infrared (FTIR) spectrometer confirmed the successful sintering of SO_4^{2-} and ligating with TiO_2 for preparing TiO_2/SO_4^{2-}. The effects of the photocatalyst were further excited by the irradiation of ultraviolet light. The highest weight percentage of glycerine acetate was obtained under a reaction time and reaction temperature of 10 h and 120 °C, respectively. In addition, it was observed that the glycerol conversion ratio reached 98.65% and the triacylglycerols compound amounted to 40.41 wt.% when the reacting molar ratio was 8. Moreover, the freezing point of the product mixture of glycerine acetate under the same molar ratio reached as low as −46.36 °C; the lowest among the products made using various molar ratios of acetic acid/glycerol. The UV light irradiation rendered higher triacylglycerols and diacylglycerols with lower diacylglycerol formation ratios than those without light irradiation.

Keywords: antifreeze; glycerine acetate; heterogeneous sulfated acid photocatalyst; esterification of bioglycerol; cosolvent

Citation: Lin, C.-Y.; Chen, Y.-C. Effects of Heterogeneous Sulfated Acid Photocatalysts and Irradiation of Ultraviolet Light on the Chemical Conversion and Characteristics of Antifreeze from Bioglycerol. *Processes* **2024**, *12*, 383. https://doi.org/10.3390/pr12020383

Academic Editors: Eleonora Aneggi and Daniele Zuccaccia

Received: 24 January 2024
Revised: 4 February 2024
Accepted: 10 February 2024
Published: 14 February 2024

1. Introduction

For every 1000 kg of biodiesel, 100 kg of its by-product of crude bioglycerol is made [1] after the transesterification reaction for biodiesel manufacture from triglyceride compounds in vegetable oils, animal fats, or microalgae lipids. Biodiesel can be produced from non-edible feedstocks such as rubber seed oil, assisted by mechanical stirring, ultrasound, or forms of microwave irradiation such as hydrodynamic cavitation reactors, mechanical stirring reactors [2], etc. The recovery of crude glycerol is problematic because it is produced from various raw materials composed of complex fatty acid mixtures. Impurities after biodiesel production include alkaline soaps, sodium hydroxide, methanol, trace elements, water, etc. [3], depending on the catalyst and feedstocks used. The prices of crude glycerol are estimated to be 200–260 USD/ton and 480–530 USD/ton for pure glycerol in Europe [4]. The annual production of crude glycerol is expected to reach 300 million tons in 2025 [5]. However, it only consumes less than 5 million tons of glycerol annually [6]. This excess glycerol production leads to a significant drop in its price. More efforts should be made, for example, by applying thermochemical or biological approaches to transform bioglycerol into more economical products. Glycerol has been used to derive other value-added pharmaceuticals or fuel additives to promote the competitiveness of whole-biodiesel products in traditional fuel markets [7]. For example, glycerol can be converted to derivatives

such as hydrogen, ethers, pharmaceuticals, glycerol esters, etc. Due to the inferior fluidity characteristics of biodiesel, its high cold filter plugging point (CFPP) causes poor drivability and even shut down of vehicle engines in cold-weather regions [8]. An effective antifreeze agent added to biodiesel can improve its low-temperature fluidity and thus vehicle drivability, especially in cold-weather environments. A high value of glycerol carbonate can be produced from the transesterification of glycerol with dimethyl carbonate (DMC) catalyzed by a heterogeneous catalyst Li/TiO_2, which is prepared via a wetness impregnation method. The highest conversion ratio of glycerol carbonate achieved was 95.5%, with a selectivity of 95.9% [9].

Glycerine acetate, which plays the role of an antifreeze agent [10], can be chemically converted from bioglycerol to reach both goals of increasing glycerol's economic value and reducing the biodiesel's CFPP. Bioglycerol can be esterified with acetic acid to form monoacylglycerols (MAG), diacylglycerols (DAG), and triacylglycerols (TAG) [11]. MAG can be used as a food additive, while DAG and TAG have been applied as gasoline anti-knocking additives and additives for reducing fuel viscosity and cold filter plugging points. In addition, the blend of MAG, DAG, and TAG can be used as printing ink, softening agents, and plasticizers [12]. In the compound mixture of glycerine acetate, the freezing points of triacylglycerols, diacylglycerols, and monoacylglycerols are as low as −78 °C, −30 °C, and −10 °C [13], respectively. Glycerol can also be converted to allyl acetate and acetal acetates through a catalytic process of deoxydehydration (DODH)/acetylation and acetylation/acetalization catalyzed using Amberlyst-15 as the heterogeneous catalyst. The yields of those products can reach 95 and 78%, respectively [14]. TAG, a transparent liquid, can be used as a plasticizer to increase the mechanical properties and crystallinity extent [15]. Triacetin and polyglycidyl nitrate (PGN) are also produced from glycerol conversion. Triacetain can be used as a bioadditive to boost the octane number of liquid fuel and enhance engine performance. PGN is the most energetic polymer to consist of a propellant binder [16].

Homogeneous or single-phase catalysts have the advantages of mild reaction conditions, high catalytic activity, and high selectivity in chemical processes [17]. However, at high temperatures, those single-phase catalysts frequently cause more unstable reactions, rigid separation of the products from the catalyst, and more difficulty in recovering the catalyst from the product mixture [18]. The release of the used single-phase catalyst after the chemical reaction might harm the environment and increase the amount of the catalyst consumed. In contrast, the advantages of heterogeneous catalysts include excellent thermal and mechanical stability, easy separation of catalysts from the products, a high extent of recovery for re-use, lower environmental pollution, and multiple use of the catalysts to reduce costs [19].

Catalysts that can accelerate photochemical reactions are called photocatalysts, the principle of which is like that of catalysts, except that photocatalysts require ultraviolet light irradiation to produce reduction or oxidation reactions with foreign substances attached to the object's surface. There are many photocatalytic materials, such as zinc oxide (ZnO), titanium dioxide (TiO_2), tin dioxide (SnO_2), cadmium sulfide (CdS), etc. Among all these materials, titanium dioxide has a more vital oxidation–reduction ability, long-lasting effects, and cheap, easy-to-obtain advantages [20]. At present, most photocatalytic materials are mainly made of titanium dioxide. Titanium dioxide has excellent physical, chemical, and thermal stability, is finely hydrophilic, has a high refractive index, and is non-toxic. It can directly contact food, so it is widely used in photocatalysts, textiles, anti-UV materials, inks, and food packaging materials [21]. As a photocatalyst material, it has the advantages of anti-abrasion, safety, and durability. There are three stable phases of titanium dioxide: slate titanium, anatase, and rutile. The latter two phases are familiar crystal structures. Titanium dioxide is entirely insulated at room temperature but will change to a semiconductor when heated or irradiated by light at specific wavelengths. Moreover, titanium dioxide (TiO_2) acts as a catalyst carrier and has a large number of pores and holes with a large surface area which can absorb a large amount of strong acid or alkaline compounds to facilitate

the esterification reaction of glycerol. Among these compounds, acid catalysts such as sulfuric acid, sodium hydrogen sulfate, *p*-toluene sulfonic acid, and methane sulfonic acid are the most used ones to facilitate the esterification reaction [22]. Shera Farisya et al. [23] synthesized a solid acid catalyst to catalyze glycerol acetylation to form acetins. They found that the increase in sulfuric acid concentration increased the number of active sites and strong acid strength, leading to the high glycerol conversion and selectivity of triacetin. When the impregnating method is used to produce a combined catalyst of TiO_2 and sulfuric acid, the carrier TiO_2 is wholly immersed in the sulfuric acid solution so that sulfuric acid is diffused to the interior surface of the pores of TiO_2. The aqueous combined catalyst of TiO_2/SO_4^{2-} is then filtered, dried, and calcinated at elevated temperatures to fix the content of sulfuric acid firmly onto the interior surfaces of all pores of TiO_2.

Titanium dioxide in the anatase crystallographic phase has the highest photocatalytic activity because of its high specific surface area and complex crystalline microstructure, inhibiting the recombination of the electron hole pair [24]. When a titanium dioxide photocatalyst is irradiated by light, which bears a larger energy gap width than the titanium dioxide, the electrons will jump from the valence band to the conductivity band, generating an electron–electron hole pair. The electron hole has oxidizing characteristics, and the electron has reducing ones. The electron will combine with oxygen molecules to form superoxide ions (O^{2-}), while the electron hole will react with OH^- on the surface of titanium dioxide to form highly oxidizing OH^- radicals. The superoxide ions and reactive OH^- radicals will decompose organic matter, leading to the enhancement of the catalytic activity of the strong acid SO_4^{2-} catalyst and acceleration of the esterification reaction of glycerol in turn. The adherence of SO_4^{2-} to TiO_2 can increase the charge separation efficiency to facilitate the production of oxidizing agents, including hydroxyl radicals [25]. Hence, the photocatalytic activity of TiO_2/SO_4^{2-} is greatly improved. Regarding the light source, the gap between the conductive band and the valence band of titanium dioxide of the anatase phase is about 3.2 eV [26]. Hence, a UV light source with a wavelength less than 387.5 nm must be provided to excite the electrons of titanium dioxide from the valence band to the conductive band and facilitate titanium dioxide to incur a photocatalytic reaction [27]. TiO_2/SO_4^{2-} photocatalysts have superior chemical and thermal stability. The careless disposal of these catalysts might not cause significant harm to the environment. A heterogeneous phase of this catalyst is prepared in this study to catalyze the esterification of glycerol. Hence, the TiO_2/SO_4^{2-} photocatalyst is prone to be separated from the reactant mixture and recycled. The photocatalyst is thus considered to have high environmental benefits. Geetha et al. [28] used a TiO_2/SO_4^{2-} photocatalyst to catalyze piperidine synthesis five times. The product yield only decreased by 2%.

Acetic acid-based glycerides can be produced through the esterification reaction of glycerol and acetic acid with an acid catalyst [29]. Nda-Umar et al. [30] used different heterogeneous catalysts such as K-10 montmorillonite, niobic acid, H form of zeolite Socony Mobil-5 (HZSM-5), H form of ultra-stable Y zeolite (HUSY), and Amberlyst-15 to catalyze the reaction of acetic acid and glycerol. Amberlyst-15 was the most active catalyst, with the highest response rate of 97% [31]. The reaction was catalyzed via Dodecamolybdophosphoric acid (PMo) sintering on the surface of NaUSY (ultra-stable Y type) zeolite for 30 min. Comparing the selectivity and yield of sintering different weights (from 0.6–5.4 wt.%) of PMo on NaUSY zeolite, in the best condition, sintering 1.6 wt.% of PMo on NaUSY zeolite for 3 h, the rate of glycerol conversion reached 68%, and the yields of MAG, DAG, and TAG achieved 37%, 59%, and 2%, respectively [32]. The sintering of PMo with weight ratios that are too high on NaUSY zeolite may result in reduced catalytic activity due to the limitation of internal diffusion [33]. Caballero et al. [34] performed the reaction of glycerol and acetic acid using Amberlyst-15 as a catalyst to achieve a more than 95% yield of glycerol triacetate at a reaction temperature of 80 °C. Sedghi et al. [35] found that a 35% yield of glycerol triacetate was converted from the reaction of glycerol with acetic acid at a reaction pressure of 1070 kPa, a reaction temperature of 160 °C, and a molar ratio of acetic acid/glycerol equal to 4. Faruque et al. [36] used a solid-state superacid catalyst, SO_4^{2-}/ZrO_2 to esterify

glycerol with acetic acid. They observed that glycerol triacetate could be yielded in a short time. Banu et al. [37] investigated the esterification of liquid-phase glycerol with acetic acid, which was catalyzed by the commercial ion exchange resin of Purolite CT-275. The molar ratios of acetic acid to glycerol were set to between 4 and 9, and reaction temperatures were between 70 and 110 °C.

TAG and DAG are recognized as biofuel additives that improve low-temperature fluidity and viscosity-reduction properties, increase octane numbers, and reduce fuel turbidity and greenhouse gas emissions [38]. The conversion of bioglycerol to produce glycerine acetate is affected by the reaction time and temperature, the molar ratio of acetic acid to bioglycerol, and the types of catalyst used. In particular, irradiated photocatalysts might alter the fuel composition distribution and, thus, their fuel characteristics. The production from bioglycerol conversion would be facilitated by irradiation of the photocatalyst. However, the catalyst characteristics of the photocatalyst TiO_2/SO_4^{2-} using techniques such as thermogravimetric analysis (TGA), Fourier transformation infrared (FTIR) spectrometry [39], and converted product distribution, as well as the weight percentage of the chemically converted antifreeze, have yet to be thoroughly investigated. The esterification reaction of glycerol with acetic acid under ultraviolet light irradiation also has yet to be quantitively analyzed based on its conversion extent from glycerol [40]. The effects of the molar ratio of acetic acid/glycerol and reacting conditions on the converted product distribution of MAG, DAG, and TAG from a glycerol and acetic acid reaction under ultraviolet light irradiation also have yet to be studied [40]. Hence, the effects of the conversion parameters of bioglycerol, such as the reaction time, temperature, and irradiation of ultraviolet light, on the catalytic characteristics of the photocatalyst TiO_2/SO_4^{2-} are evaluated using techniques such as TGA and FTIR. Additionally, the properties of the formed antifreeze product of glycerine acetate are investigated in this study.

2. Materials and Methods

Titanium dioxide (TiO_2) powder of a nanometer (nm) size was acidified using sulfuric acid to form a solid-state strong acid photocatalyst. The TiO_2/SO_4^{2-} photocatalyst catalyzed the reaction of glycerol with acetic acid to facilitate the formation of acetic acid-based glycerides. The catalyst characteristics and glyceride fuel properties were analyzed to find the optimum reacting conditions for the products. The catalyst and glyceride preparation methods and analysis procedures are explained below.

2.1. Preparation for Heterogeneous Strong Acid Photocatalysts and Acetic Acid-Based Glycerides

2.1.1. Preparation of TiO_2/SO_4^{2-} Solid-State Strong Acid Photocatalyst

In this experiment, titanium dioxide powder was immersed in a dilute sulfuric acid solution for 24 h and then filtered and forged at high temperatures to obtain the TiO_2/SO_4^{2-} photocatalyst. The purified titanium dioxide powder was filtered using a vacuum pump and poured into a ceramic beaker. The powder was then heated based on the set temperature control program of the high-temperature furnace, baked at 100 °C for 4 h, and then forged at 450 °C for 3 h. The sample was then taken out, cooled down naturally, and ground.

2.1.2. Preparation of Acetic Acid-Based Glycerides

Bioglycerol and acetic acid were poured into a three-necked round-bottom flask, then TiO_2/SO_4^{2-}, a heterogeneous strong-acid photocatalyst, was added. The reactant mixture was heated using a temperature-controlled magnetic stirrer until it reached a preset temperature. The intake air pump and the ultraviolet (UV) light of LED (light-emitting diode) lamps (Midas Technology Corp., New Taipei City, Taiwan) at the port were triggered simultaneously to irradiate the TiO_2/SO_4^{2-} solid-state strong acid photocatalyst. The wavelengths of the LED lamp were in the range of 320 to 380 nm. Moisture was produced during the esterification reaction and accumulated in a collecting tank. The experimental setup for manufacturing the antifreeze glycerine acetate is illustrated in Figure 1. At the first testing stage, the photocatalyst was prepared at a reaction temperature of 120 °C, a time of 10 h, acetic

acid/glycerol molar ratios from 5 to 9, and a photocatalyst of 4 wt.% of the reacting glycerol. The appropriate molar ratio of acetic acid/glycerol was selected to prepare the photocatalyst. The optimum molar ratio for the photocatalyst production was determined based on the characteristics of the photocatalyst. The difference in the photocatalyst's characteristics after being irradiated by a UV 6 W LED light was compared with the no irradiation condition. In the second stage, a reaction temperature of 100 °C, pressure of 55 kPa, acetic acid/glycerol molar ratios from 5 to 9, and reaction time of 6 h were set. The UV power varied from 1 W to 6 W. The optimum preparation conditions were selected according to the properties of the acetic acid-based glycerides converted from the esterification reaction of glycerol.

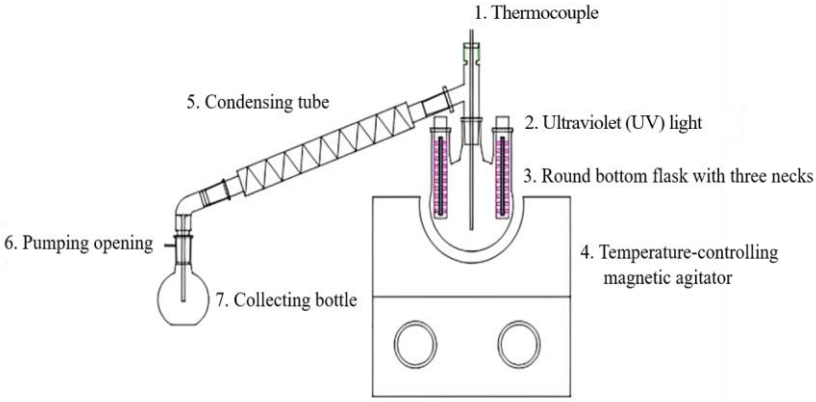

Figure 1. Experimental set-up for producing glycerine acetate from the esterification reaction of glycerol and acetic acid.

2.1.3. After-Treatment Procedures for the Prepared Glycerine Acetate Product

The esterified product obtained from the reaction of glycerol with acetic acid, which was assisted with the catalytic effects of TiO_2/SO_4^{2-} solid-state strong acid photocatalyst, required further after-treatment processing to enhance its purity. After the reaction, the catalyst was removed using a centrifuging separator, which spun for 20 min at 4500 rpm. After being centrifuged out of the catalyst and other impurities, the product was filtered through a glass fiber filter paper, followed by a process of vacuum distillation at 105 °C to distill away the excess water and acetic acid until no more condensed liquid droplets appeared. The sample was then titrated using an acid-value titrator (model 785DMP Titrino, Metrohm Ltd., Herisau, Switzerland) to indicate the amount of acetic acid contained in the sample, which was then neutralized with the same molarity of sodium hydroxide. Finally, a gas chromatography–mass spectrometer (GC-MS) was used to analyze the composition and compound distribution of the sample so that the optimum experimental conditions could be adjusted to obtain superior fuel characteristics. GC-MS analysis might not be sensitive enough for certain compounds such as some herbicides, but it is sensitive to the analysis of most organic matters.

2.2. Analysis of Characteristics of Solid-State Strong Acid Photocatalysts and Glycerine Acetate

2.2.1. TiO_2/SO_4^{2-} Heterogeneous Strong Acid Photocatalyst Characterization

A high-resolution X-ray photoelectron spectrometer (XPS) was used to examine the effects of the sintered sulfuric acid on the crystal structure of titanium dioxide (TiO_2). The XPS appears to yield high-quality measurements when it is applied to the analysis of homogeneous solid materials. An X-ray diffractometer (XRD, Model TRAX III), a product of the Rigaku Corporation, Japan, was used to measure the catalyst at either a wide or low sweeping angle. The XRD analysis does not apply to those amorphous materials whose structures do not have the long-range order of atomic arrangements in the crystal structure. A Fourier transform infrared spectrometer (FTIR, Model Tensor 27), a product of Bruker Ltd., Berlin, Germany, uses interference spectroscopy for Fourier transformation to obtain vibrational spectra of compounds so that organic, inorganic, or biochemical molecules

can be identified. The FTIR spectra were used to determine the molecular structure of the product samples and the catalyst before and after being sintered. The FTIR analysis is limited to the discrete Fourier transform because the variation between the successive phase differences is fixed.

2.2.2. Characteristics Analysis of Glycerine Acetate

A gas chromatography-mass spectrometer is composed of two different instruments. The gas chromatograph (model JMS-700, JEOL Ltd., Tokyo, Japan) separates mixtures into pure substances, using various components in a fixed liquid phase or mobile gas phase due to the difference in the distribution rate to achieve the effect of separation. The mass spectrometer (model QP2010, Shimadzu Ltd., Kyoto, Japan), connected to the gas chromatograph, can determine the molecular weight and structure of the analyzed compound. Because electrons irradiate the sample in the free chamber of the mass spectrometer, the compounds are frozen and cracked. The electric field and bending magnetic field accelerate the positively charged fragments or ions to obtain the mass spectra.

3. Results and Discussion

3.1. Characterization of the Heterogeneous Strong Acid Photocatalyst

The crystalline structure and attached sulfur oxides of the TiO_2/SO_4^{2-} solid-state strong acid photocatalyst were analyzed using an infrared powder diffractometer, infrared spectrometer, and thermogravimetric analysis. The results are discussed as follows.

3.1.1. Structural Analysis of the TiO_2/SO_4^{2-} Photocatalyst

In this experiment, the TiO_2/SO_4^{2-} photocatalyst was analyzed using an infrared powder diffractometer. The heterogeneous TiO_2/SO_4^{2-} photocatalyst prepared in this experiment does not affect the chemical structure of TiO_2 itself [41] due to the presence of SO_4^{2-} in the range of the 2θ angle scanned from 20° to 80°, as shown in Figure 2. Hence, the structure of the X-ray intensity between the catalysts of TiO_2 and the TiO_2/SO_4^{2-} photocatalyst are similar, corresponding to the scanned 2θ angle in Figure 2.

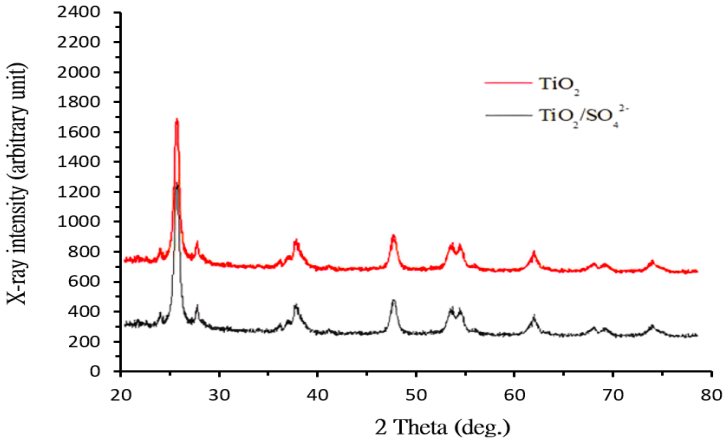

Figure 2. Comparison of X-ray intensity between the TiO_2/SO_4^{2-} and TiO_2 catalysts.

3.1.2. Analysis of Infrared Spectroscopy for the TiO_2/SO_4^{2-} Photocatalyst

According to Wang et al. [42], the most common binding modes of SO_4^{2-} and metal oxides are bridging and chelating types. The infrared spectra formed by the SO vibrations in SO_4^{2-} are different for different binding modes. The chelating coordination, which was in the ranges of 940~960, 1035~995, 1125~1090, and 1240~1030 cm^{-1}, belonged to the anti-symmetric and symmetric vibrational peaks of S=O and S-O, respectively.

Shihab et al. [43] confirmed that the highest amplitude of vibration of the chelating ligand in the compound is higher than that of the bridging ligand. Moreover, the SO_4^{2-} in the catalyst is bound to the substrate through the chelating ligand. The SO_4^{2-}-chelating ligand

can strongly attract electrons in the substrate to produce an intense acid reaction [44]. The Fourier transform infrared spectroscopy (FTIR) analysis of the TiO_2/SO_4^{2-} photocatalyst and TiO_2 catalyst is shown in Figure 3.

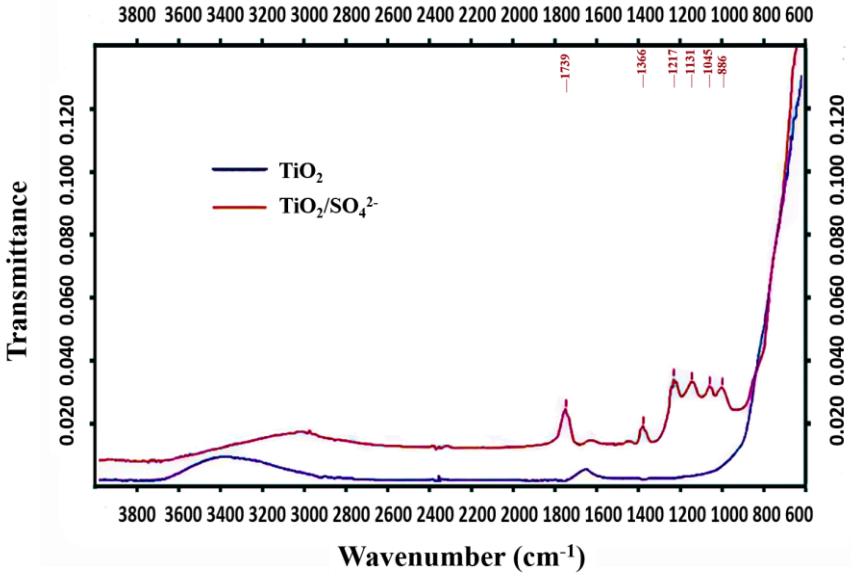

Figure 3. Comparison of the Fourier transform infrared spectrometer (FTIR) analysis for the TiO_2/SO_4^{2-} and TiO_2 catalysts.

The absorption peaks in the range of 1300~900 cm^{-1} are the characteristic vibrational peaks of the SO_4^{2-} in TiO_2/SO_4^{2-}. The infrared spectrometer demonstrated that the different bonding modes of sulfur oxides on TiO_2 are different, but still in the range of 1300~900 cm^{-1}. In Figure 3, 1366 and 1739 cm^{-1} are at the bending vibration and absorption peaks of bonded water-OH, where the absorption peaks at 986 cm^{-1} belong to the symmetrically stretching vibration and absorption peaks of the S-O single bond. In contrast, the absorption peaks at 1045 and 1131 cm^{-1} belong to S=O [45]. Therefore, it is inferred that the heterogeneous strong acid TiO_2/SO_4^{2-} photocatalyst prepared in this experiment appeared to cause sintering of SO_4^{2-} on the carriers, where it ligated with TiO_2.

3.1.3. Thermogravimetric Analysis of the TiO_2/SO_4^{2-} Photocatalyst

Figure 4 shows the thermogravimetric analysis (TGA) results for the photocatalysts TiO_2/SO_4^{2-} and TiO_2. The weight loss peaks around 200 and 300 °C, corresponding to free and crystalline water removal, respectively, for the heterogeneous strong acid TiO_2/SO_4^{2-} photocatalyst. The weight loss of the catalyst is mainly caused by the water loss due to water adsorption onto the catalyst [46]. The new weight loss peak at 540 °C was attributed to the loss of SO_4^{2-} due to decomposition of SO_4^{2-} from the TiO_2/SO_4^{2-} photocatalyst, agreeing with the findings of Vargas-Villanueva et al. [47].

3.2. Effects of Molar Ratio on Product Compositions Converted from Glycerol

The chemical conversion conditions of glycerol included the molar ratios of acetic acid/glycerol equal to from 5 to 9, reaction temperature of 120 °C, and reaction time of 10 h. A 4 wt.% heterogeneous strong acid catalyst of glycerol was used to produce glycerine acetate. The product characteristics derived from the conversion reaction from glycerol catalyzed with the TiO_2/SO_4^{2-} catalyst were compared during chemical reactions assisted with or without UV light irradiation. The power of the LED (light-emitting diode) light lamp for the irradiation was set to 120 mW. The optimum preparation conditions, such as the molar ratios of acetic acid/glycerol, reaction time, and amount of the catalyst, etc. were determined accordingly.

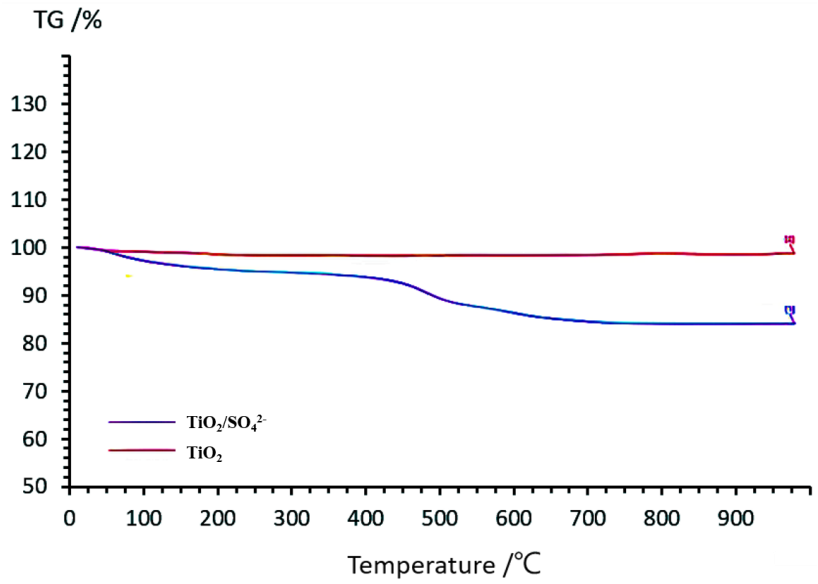

Figure 4. Comparison of TGA (thermogravimetric analysis) between the TiO_2/SO_4^{2-} and TiO_2 catalysts.

3.2.1. Effect of Irradiated UV Light and Molar Ratio on the Conversion Ratio of Glycerol

The effects of the acetic acid/glycerol molar ratio on the conversion ratio of glycerol under different preparation conditions were analyzed using gas phase chromatography. As shown in Figure 5, under UV light irradiation of LED lamps on the catalyst surface, the conversion ratio of glycerol increased with increases in the molar ratio of acetic acid/glycerol, especially at a molar ratio equal to 8. The conversion ratio of glycerol to glycerine acetate under this molar ratio reached 98.65%. However, the conversion ratio of glycerol decreased with increases in the molar ratio of acetic acid/glycerol when the molar ratio was larger than 9.

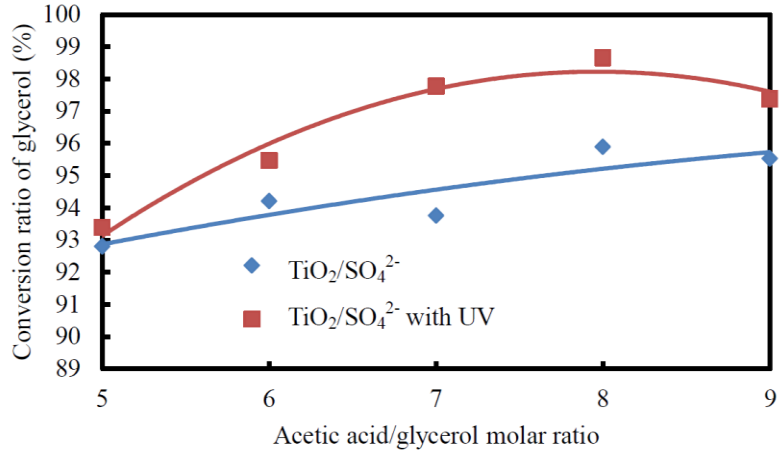

Figure 5. Effects of ultraviolet (UV) light irradiation and the acetic acid/glycerol molar ratio on the conversion ratio of glycerol (%).

The conversion ratio of glycerol was significantly higher because the concentration of glycerol in the reaction mixture of glycerol and acetic acid is one of the major conversion factors. The lower viscosity of the reactant mixture involving a larger ratio of acetic acid to glycerol facilitated the esterification reaction of glycerol [48]. However, the conversion ratio decreased when the molar ratio exceeded 9, mainly because too much acetic acid diluted the glycerol concentration, leading to a lower conversion ratio [49]. The glycerol conversion ratio under the UV light irradiation using LED lamps decreased to 98.03% at a molar ratio equal to 9. The optimum molar ratio of acetic acid/glycerol was found to be

8. Adequate amounts of glycerol and acetic acid are required to obtain a high conversion ratio of glycerine acetate from glycerol.

Acetic acid will accept a proton (H^+) to react with glycerol during the esterification reaction. A dehydration condensation reaction might occur, leading to the formation of H_2O [50]. When UV light from the LED lamps is irradiated onto the heterogeneous strong acid photocatalyst surface, the TiO_2 photocatalyst will generate an electron–electron hole (e^--p^+) pair. The electron hole (p^+) and H_2O attached to the photocatalyst surface will produce H^+ and OH^- [51], increasing the H^+ in the reaction environment. Acetic acid is also prone to receiving H^+ to react with glycerol. Therefore, heterogeneous strong acid photocatalysts will accelerate the conversion ratio of glycerol and acetic acid under UV light irradiation in the same reaction environment.

3.2.2. Effects of UV Light Irradiation and Molar Ratio on Triacylglycerol Production

Figure 6 shows the effects of the heterogeneous strong acid photocatalyst TiO_2/SO_4^{2-} on the catalytic conversion from glycerol to triacylglycerol (TAG) under UV light and varied molar ratios. The selectivity of triacylglycerols increased significantly by increasing the acetic acid/glycerol molar ratio and UV light irradiation of LED lamps on the photocatalyst surface.

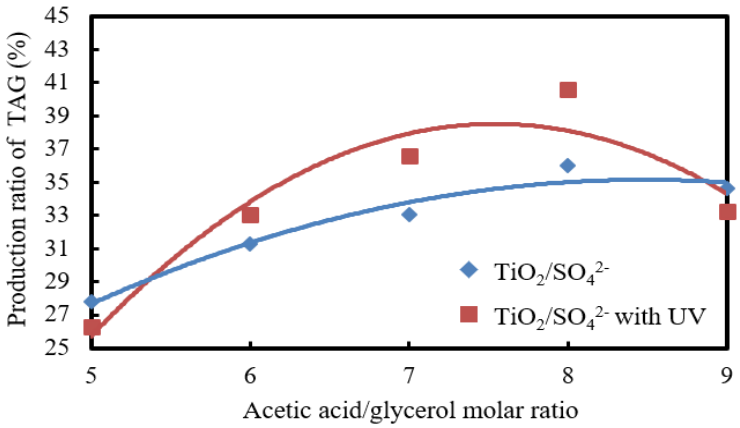

Figure 6. Effects UV light irradiation and acetic acid/glycerol molar ratio on the production ratio (wt.%) of TAG in the glycerine acetate product.

A larger molar ratio of acetic acid/glycerol caused more intense reactions and increased production of triacylglycerols (TAG). The molar ratio is a more critical factor affecting glycerol conversion into triacylglycerol, which is the final product of the conversion process. The hydroxyl group (OH^-) in the glycerol molecule and the carboxyl group (-COOH) in the acetic acid molecule first proceeded through a dehydration condensation reaction to produce monoacylglycerols (MAG). The monoacylglycerols further underwent a dehydration condensation reaction with the acetic acid's carboxyl group (-COOH) to form diacylglycerol (DAG). Since the hydroxyl group (OH^-) has less spatial resistance than the carboxyl group (-COOH), it hinders the occurrence of a dehydration condensation reaction between OH^- in diacylglycerol and -COOH in acetic acid molecules [52]. Hence, the production of triacylglycerol is more complex than that of diacylglycerol and monoacylglycerol. Therefore, the higher the acetic acid/glycerol molar ratio, the more triacylglycerols are produced. When the molar ratio of acetic acid to glycerol reached 8, the highest formation ratio of triacylglycerols appeared, which was 40.41 wt.%. However, after the acetic acid/glycerol molar ratio exceeded 8, the effects of the acetic acid/glycerol molar ratio on the yield of triacylglycerols decreased for the case of UV irradiation on the photocatalyst surface shown in Figure 6. The production ratio significantly decreased to 34.63% when a molar ratio equal to 9 was used.

When the heterogeneous strong acid photocatalyst was irradiated with UV light, the photoexcitation generated an electron–electron hole pair, resulting in a photocatalytic

reaction. When the solid-state strong acid photocatalyst is subjected to energy of an appropriate amount, the electrons are excited by the light energy and jump up from the valence band to the conduction band. The valence band forms an unfilled vacancy called an electron hole. The electron and electron hole that jump to the conduction band are called an electron–electron hole pair [53]. In the esterification reaction of glycerol and acetic acid, water is produced during the dehydration condensation reaction. When the electron hole attaches to the nearby water molecules, H^+ and OH^- are produced, resulting in more H^+. Meanwhile, acetic acid is more receptive to H^+ to react with glycerol. Consequently, the reaction rate increases, causing a higher production rate of triacylglycerol.

The highest production amount of triacylglycerol was 40.41% at a molar ratio of acetic acid/glycerol equal to 8. The freezing point of triacylglycerol is −78 °C. Hence, 8 is the optimum molar ratio to convert glycerol to form a superior antifreeze agent with the lowest freezing point, which was −46.36 °C among the acetyl glyceride products made from various molar ratios in the range of 5 to 9. The highest weight percentage of triacylglycerol in the glycerine acetate was also considered to be an excellent mixture of the converted product from glycerol.

3.2.3. Effects of Irradiated UV Light and Molar Ratio on Diacylglycerol Production

Figure 7 shows the effects of the molar ratio of acetic acid/glycerol and UV light irradiation on the formation of diacylglycerol (DAG), which were analyzed using a gas chromatography analyzer. Under UV light irradiation, the diacylglycerol content was significantly larger than that produced under no UV light irradiation. The highest diacylglycerol content, which amounted to 56.04%, occurred at a molar ratio of 5 under UV light irradiation, while the content of diacylglycerols did not significantly change with variations in the molar ratio without UV-light irradiation.

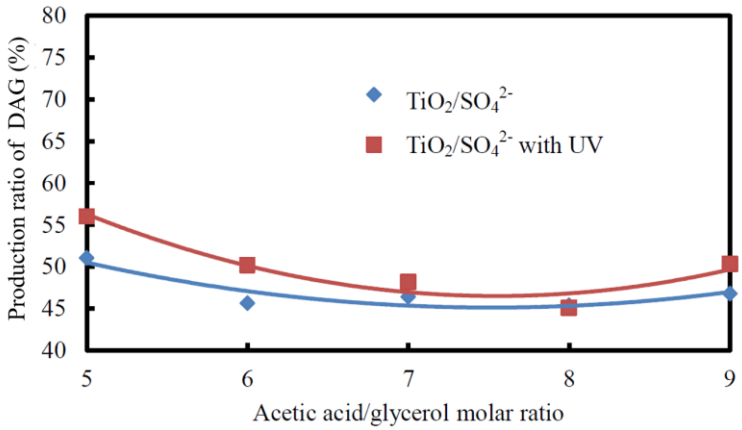

Figure 7. Effects of UV light irradiation and acetic acid/glycerol molar ratio on the DAG production ratio (wt.%).

Diacylglycerols are formed when the OH^- radicals of monoacylglycerols (MAG) react with the -COOH of acetic acid in a dehydration condensation reaction [54]. The effect of the acetic acid/glycerol molar ratio was not significant for the formation of diacylglycerols. The increase in the acetic acid concentration in the reactant mixture further drives the transesterification equilibrium of converting monoacylglycerols into diacylglycerols and triacylglycerols [55]. The acetic acid content is low when a low acetic acid/glycerol molar ratio is set. It is inferred that due to the low acetic acid content, there is not enough acetic acid to facilitate the reaction of glycerol with diacylglycerols to form triacylglycerols. Therefore, at a molar ratio of 5 and under UV-light irradiation, the content of diacylglycerols reached the highest among various molar ratios shown in Figure 7.

When UV light from LED lamps irradiates the solid-state strong acid photocatalyst, the electrons receive enough power to jump from the valence band to the conduction band, forming a positively charged electron–electron hole pair. A positively charged electron hole

will be created simultaneously where the original electrons exist. The electron hole has oxidizing effects. Hence, water molecules will be oxidized to produce OH^- and H^+ [56]. The increase in H^+ radicals in the acetic acid accelerates its reaction with glycerol. In consequence, the conversion rate of glycerol increases to produce more diacylglycerol within the same reaction time.

3.2.4. Effects of Irradiated UV Light and Molar Ratio on Monoacylglycerol Production

The effects of the acetic acid/glycerol molar ratio and UV light irradiation on monoacylglycerol (MAG) formation are shown in Figure 8. There was no apparent variation in the monoacylglycerol content with the acetic acid/glycerol molar ratio under no LED UV light irradiation. However, a higher amount of monoacylglycerol formation without UV light irradiation compared to that with UV-light irradiation was observed. There was a slight increase in the monoacylglycerol content with the rise in the acetic acid/glycerol molar ratio when the UV light irradiated the catalyst surface. The highest formation ratio of monoacylglycerol, which was 13.67%, occurred when the molar ratio of acetic acid/glycerol was equal to 9. In addition, at the same molar ratio, the monoacylglycerol formation between the cases with and without UV light irradiation reached nearly the same level.

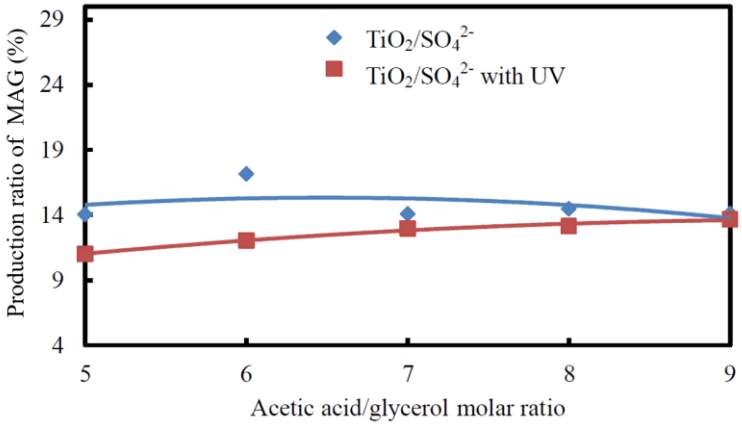

Figure 8. Effects of ultraviolet (UV) light irradiation and the acetic acid/glycerol molar ratio on the production ratio (wt.%) of MAG in the product.

The variation in monoacylglycerol production with the acetic acid/glycerol molar ratio was insignificant due to the high extent of complete glycerol conversion after a long reaction time of 10 h. The UV light irradiation accelerated the monoacylglycerol conversion process to produce diacylglycerol and triacylglycerol. Hence, when the glycerol reaction was exposed to UV light irradiation, it resulted in significantly less monoacylglycerol formation than when glycerol conversion occurred without UV light irradiation. This implies that the UV-light irradiation played a role in enhancing the glycerol conversion processes.

4. Conclusions

1. The TiO_2/SO_4^{2-} heterogeneous strong acid photocatalyst prepared in this experiment did not affect the crystalline phase of TiO_2 itself under the presence of SO_4^{2-}, nor did it affect the symbolic wavelength of the crystalline structure of TiO_2 of the sharp titanium type. Hence, similar X-ray intensity structures between the catalysts of TiO_2 and TiO_2/SO_4^{2-} were observed.
2. The presence of bonding wavelengths of sulfur oxide in the infrared spectral frequency between 900 and 1300 cm^{-1} was confirmed using Fourier-transform infrared spectroscopy (FTIR). The experimental observance also confirmed that preparing the heterogeneous strong acid photocatalysts was effective in sintering SO_4^{2-} to its carrier and bonding it with TiO_2.

3. In comparison with the TiO_2 catalyst analyzed via thermogravimetric analysis, the TiO_2/SO_4^{2-} catalyst was found to have significant weight loss at 540 °C because of the decomposition of SO_4^{2-}.
4. The glycerol conversion ratio reached 98.65% under the reaction conditions of a molar ratio of acetic acid/glycerol equal to 8, a reaction temperature of 120 °C, a UV light wavelength of 365 nm, and a reaction time of 10 h. The derived product of glycerine acetate under the above conversion conditions appeared to have superior antifreeze properties, including the lowest freezing point, which was −46.36 °C. In addition, the content of triacylglycerol in the product under the above reaction conditions was the highest, 40.41%.
5. When the molar ratio of acetic acid/glycerol was increased to 9, the glycerol conversion rate and the formation of glycerol triacetate in the product decreased to 98.03% and 34.63%, respectively, under the application of UV-light irradiation on the catalyst.
6. The highest formation ratios of diacylglycerol and monoacylglycerol, which were 56.04% and 13.67%, respectively, appeared at molar ratios of acetic acid/glycerol equal to 5 and 9, respectively. In addition, the formation ratio of monoacylglycerol at a molar ratio equal to 9 converged for the cases with and without UV light irradiation.
7. The effects of UV light irradiation on the TiO_2/SO_4^{2-} photocatalyst for the esterification reaction of glycerol with acetic acid caused higher triacylglycerol and diacylglycerol formation and lower monoacylglycerol formation than the reactions occurring without UV light irradiation.

Author Contributions: Conceptualization, C.-Y.L.; methodology, C.-Y.L.; formal analysis, Y.-C.C.; investigation, C.-Y.L.; data curation, Y.-C.C.; writing—original draft preparation, C.-Y.L. and Y.-C.C.; writing—review and editing, C.-Y.L.; supervision, C.-Y.L.; project administration, C.-Y.L. All authors have read and agreed to the published version of the manuscript.

Funding: This research was funded by the National Science and Technology Council, Taiwan, under contract number NSTC 109-2221-E-019-024.

Institutional Review Board Statement: Not applicable.

Informed Consent Statement: Not applicable.

Data Availability Statement: The data utilized in this study are contained within this article.

Acknowledgments: The authors would like to gratefully acknowledge the financial support received from the National Science and Technology Council, Taiwan, under the contract number NSTC 109-2221-E-019-024.

Conflicts of Interest: The authors declare no conflict of interest.

References

1. Braga, E.R.; Neto, G.J.; Braga, R.R.; Pontes, L.A. Optimized conditions for the design and operation of a vacuum distillation column for the purification of crude glycerol from biodiesel production. *Biofuel. Bioprod. Biorefin.* **2023**, *17*, 1203–1220. [CrossRef]
2. Samuel, O.D.; Aigba, P.A.; Tran, T.K.; Fayaz, H.; Pastore, C.; Der, O.; Mustafa, A. Comparison of the techno-economic and environmental assessment of hydrodynamic cavitation and mechanical stirring reactors for the production of sustainable hevea Brasiliensis ethyl ester. *Sustainability* **2023**, *15*, 16287. [CrossRef]
3. Raj, J.V.A.; Kumar, R.P.; Vijayakumar, B.; Gnansounou, E.; Bharathiraja, B. Modelling and process optimization for biodiesel production from Nannochloropsis salina using artificial neural network. *Bioresour. Technol.* **2021**, *329*, 124872. [CrossRef]
4. Maina, S.; Dheskali, E.; Papapostolou, H.; Castro, A.M.d.; Guimaraes Freire, D.M.; Nychas, G.J.; Papanikolaou, S.; Kookos, I.K.; Koutinas, A. Bioprocess development for 2, 3-butanediol production from crude glycerol and conceptual process design for aqueous conversion into methyl ethyl ketone. *ACS Sustain. Chem. Eng.* **2021**, *9*, 8692–8705. [CrossRef]
5. Kumar, L.R.; Yellapu, S.K.; Tyagi, R.D.; Drogui, P. Cost, energy and GHG emission assessment for microbial biodiesel production through valorization of municipal sludge and crude glycerol. *Bioresour. Technol.* **2020**, *297*, 122404. [CrossRef]
6. Alisson Dias da Silva, R.; Ana Luíza Freitas, F.; Antônio Ésio, B.; Rita Maria de Brito, A.; Luiz Antônio Magalhães, P. *Market Prospecting and Assessment of the Economic Potential of Glycerol from Biodiesel*; IntechOpen: London, UK, 2020; pp. 185–198.
7. Moklis, M.H.; Cheng, S.; Cross, J.S. Current and Future Trends for Crude Glycerol Upgrading to High Value-Added Products. *Sustainability* **2023**, *15*, 2979. [CrossRef]

8. Lin, C.-Y. The influences of promising feedstock variability on advanced biofuel production: A review. *J. Mar. Sci. Technol.* **2022**, *29*, 714–730. [CrossRef]
9. Jaiswal, S.; Pradhan, G.; Sharma, Y.C. Green and facile synthesis of glycerol carbonate from bio-glycerol assisted by lithium titanate: A robust and selective heterogeneous catalyst. *J. Taiwan Inst. Chem. Eng.* **2021**, *128*, 388–399. [CrossRef]
10. Lima, P.J.M.; da Silva, R.M.; Neto, C.A.C.G.; Gomes e Silva, N.C.; Souza, J.E.d.S.; Nunes, Y.L.; Sousa dos Santos, J.C. An overview on the conversion of glycerol to value-added industrial products via chemical and biochemical routes. *Biotechnol. Appl. Biochem.* **2022**, *69*, 2794–2818. [CrossRef]
11. de Sousa Junior, P.G.; do Nascimento Camara, A.G.; Oliveira, A.R.T.; de Castro Lima, G.; Lima, G.V.; Coutinho, L.P.; Alexandre, J.Y.N.H.; Serafim, L.F.; de Mattos, M.C.; de Kássio Monteiro, N.V. Optimization and theoretical analysis of lipase-catalyzed enzymatic esterification of glycerol for efficient glycerides synthesis. *Biochem. Eng. J.* **2023**, *198*, 109033. [CrossRef]
12. Dizoğlu, G.; Sert, E. Fuel additive synthesis by acetylation of glycerol using activated carbon/UiO-66 composite materials. *Fuel* **2020**, *281*, 118584. [CrossRef]
13. Cheong, B.E.; Yu, D.; Martinez-Seidel, F.; Ho, W.W.H.; Rupasinghe, T.W.; Dolferus, R.; Roessner, U. The Effect of Cold Stress on the Root-Specific Lipidome of Two Wheat Varieties with Contrasting Cold Tolerance. *Plants* **2022**, *11*, 1364. [CrossRef]
14. Rigo, D.; Polidoro, D.; Marcuzzo, L.; Perosa, A.; Selva, M. Isopropenyl Acetate for the Continuous-Flow Synthesis of Triacetin, Solketal Acetate, and Allyl Acetate from Pure or Crude Glycerol. *ACS Sustain. Chem. Eng.* **2023**. [CrossRef]
15. Salas-Papayanopolos, H.; Morales-Cepeda, A.B.; Wood-Adams, P.; Sanchez, S.; Lafleur, P.G.; Vazquez, H.P. Crystallization effect of poly (L-lactic acid)/silver nanocomposites blends, on barrier and mechanical properties using glyceryl triacetate as plasticizer. *Polym. Bull.* **2023**, *80*, 5273–5290. [CrossRef]
16. Mufrodi, Z.; Astuti, E.; Budiman, A.; Prasetya, A. Utilization of glycerol from biodiesel industry by-product into several higher value products. In *Valorisation of Agro-Industrial Residues*; Springer: Berlin/Heidelberg, Germany, 2020; Volume 2, pp. 145–172. ISBN 978-3-030-39207-9.
17. Mandari, V.; Devarai, S.K. Biodiesel Production Using Homogeneous, Heterogeneous, and Enzyme Catalysts via Transesterification and Esterification Reactions: A Critical Review. *Bioenergy Res.* **2022**, *15*, 935–961. [CrossRef] [PubMed]
18. Pant, K.K.; Gupta, S.K.; Ahmad, E. *Catalysis for Clean Energy and Environmental Sustainability*; Springer: Berlin/Heidelberg, Germany, 2021; Volume 1, pp. 185–208.
19. Yu, X.; Williams, C.T. Recent advances in the applications of mesoporous silica in heterogeneous catalysis. *Catal. Sci. Technol.* **2022**, *12*, 5765–5794. [CrossRef]
20. Castro-Hoyos, A.M.; Rojas Manzano, M.A.; Maury-Ramírez, A. Challenges and opportunities of using titanium dioxide photocatalysis on cement-based materials. *Coatings* **2022**, *12*, 968. [CrossRef]
21. Ijaz, M.; Zafar, M. Titanium dioxide nanostructures as efficient photocatalyst: Progress, challenges and perspective. *Int. J. Energy Res.* **2021**, *45*, 3569–3589. [CrossRef]
22. Khan, Z.; Javed, F.; Shamair, Z.; Hafeez, A.; Fazal, T.; Aslam, A.; Rehman, F. Current developments in esterification reaction: A review on process and parameters. *J. Ind. Eng. Chem.* **2021**, *103*, 80–101. [CrossRef]
23. Shera Farisya, M.R.; Irmawati, R.; Shafizah, I.N.; Taufiq-Yap, Y.H.; Muhamad, E.N.; Lee, S.L.; Salamun, N. Assessment on the effect of sulfuric acid concentration on physicochemical properties of sulfated-titania catalyst and glycerol acetylation performance. *Catalysts* **2021**, *11*, 1542. [CrossRef]
24. de Oliveira, C.P.M.; Lage, A.L.A.; da Silva Martins, D.C.; Mohallem, N.D.S.; Viana, M.M. High surface area TiO_2 nanoparticles: Impact of carboxylporphyrin sensitizers in the photocatalytic activity. *Surf. Interfaces* **2020**, *21*, 100774. [CrossRef]
25. Nguyen, T.L.; Dinh Quoc, V.; Nguyen, T.L.; Le, T.T.T.; Dinh, T.K.; Nguyen, V.T.; Nguyen, P.H. Visible-light-driven SO_4^{2-}/TiO_2 photocatalyst synthesized from binh dinh (Vietnam) Ilmenite ore for rhodamine B degradation. *J. Nanomater.* **2021**, *2021*, 1–13. [CrossRef]
26. Skipitari, M.; Kalaitzopoulou, E.; Papadea, P.; Varemmenou, A.; Gavriil, V.E.; Sarantopoulou, E.; Cefalas, A.C.; Tsakas, S.; Rosmaraki, E.; Margiolaki, I. Titanium dioxide nanoparticle-based hydroxyl and superoxide radical production for oxidative stress biological simulations. *J. Photochem. Photobiol. A Chem.* **2023**, *435*, 114290. [CrossRef]
27. Wanniarachchi, W.C.P.; Arunasalam, T.; Ravirajan, P.; Velauthapillai, D.; Vajeeston, P. Hybrid Functional Study on Electronic and Optical Properties of the Dopants in Anatase TiO_2. *ACS Omega* **2023**, *8*, 42275–42289. [CrossRef] [PubMed]
28. Geetha, S.; Thangamani, A.; Valliappan, R.; Vedanayaki, S.; Ganapathi, A. Sulfated titania (TiO_2–SO_4^{2-}) as an efficient and reusable solid acid catalyst for the multi-component synthesis of highly functionalized piperidines. *Chem. Data Collect.* **2020**, *30*, 100565. [CrossRef]
29. Mou, R.; Wang, X.; Wang, Z.; Zhang, D.; Yin, Z.; Lv, Y.; Wei, Z. Synthesis of fuel bioadditive by esterification of glycerol with acetic acid over hydrophobic polymer-based solid acid. *Fuel* **2021**, *302*, 121175. [CrossRef]
30. Nda-Umar, U.I.; Ramli, I.B.; Muhamad, E.N.; Azri, N.; Amadi, U.F.; Taufiq-Yap, Y.H. Influence of heterogeneous catalysts and reaction parameters on the acetylation of glycerol to acetin: A review. *Appl. Sci.* **2020**, *10*, 7155. [CrossRef]
31. Jadhav, H.; Annapure, U. Greener route for intensified synthesis of Tricaprylin using Amberlyst-15. *J. Chem. Sci.* **2021**, *133*, 1–7. [CrossRef]
32. da Silva, M.J.; Lopes, N.P.G.; Rodrigues, A.A. Biodiesel Additives Synthesis Using Solid Heteropolyacid Catalysts. *Energies* **2023**, *16*, 1332. [CrossRef]

33. Pang, C.; Han, R.; Su, Y.; Zheng, Y.; Peng, M.; Liu, Q. Effect of the acid site in the catalytic degradation of volatile organic compounds: A review. *Chem. Eng. J.* **2023**, *454*, 140125. [CrossRef]
34. Caballero, K.V.; Guerrero-Amaya, H.; Baldovino-Medrano, V.G. Revisiting glycerol esterification with acetic acid over Amberlyst-35 via statistically designed experiments: Overcoming transport limitations. *Chem. Eng. Sci.* **2019**, *207*, 91–104. [CrossRef]
35. Sedghi, R.; Shahbeik, H.; Rastegari, H.; Rafiee, S.; Peng, W.; Nizami, A.S.; Gupta, V.K.; Chen, W.H.; Lam, S.S.; Pan, J. Turning biodiesel glycerol into oxygenated fuel additives and their effects on the behavior of internal combustion engines: A comprehensive systematic review. *Renew. Sustain. Energy Rev.* **2022**, *167*, 112805. [CrossRef]
36. Faruque, M.O.; Razzak, S.A.; Hossain, M.M. Application of heterogeneous catalysts for biodiesel production from microalgal oil—A review. *Catalysts* **2020**, *10*, 1025. [CrossRef]
37. Banu, I.; Bumbac, G.; Bombos, D.; Velea, S.; Gălan, A.M.; Bozga, G. Glycerol acetylation with acetic acid over Purolite CT-275. Product yields and process kinetics. *Renew. Energ.* **2020**, *148*, 548–557. [CrossRef]
38. Cai, Z.; Zhuang, X.; Yang, X.; Huang, F.; Wang, Y.; Li, Y. Litsea cubeba kernel oil as a promising new medium-chain saturated fatty acid feedstock for biolubricant base oil synthesis. *Ind. Crops Prod.* **2021**, *167*, 113564. [CrossRef]
39. Peter, A.; Nicula, C.; Mihaly Cozmuta, A.; Drazic, G.; Peñas, A.; Silvi, S.; Mihaly Cozmuta, L. Polylactic Acid-Based Film Modified with Nano-Ag-Graphene-TiO_2: New Film versus Recycled Film. *Adv. Polym. Technol.* **2023**. [CrossRef]
40. Özyiğit, B.; Sayilganlar, E.; Akbay, E. Photocatalytic esterification of acetic acid with methanol over metal-exchanged phosphotungstate. *J. Photochem. Photobiol. A Chem.* **2024**, *447*, 115280. [CrossRef]
41. Verma, P.; Wanchoo, R.K.; Toor, A.P. Plasmonic silver nanoparticles decorated surface functionalized Zirconium doped quantum dots-for enhanced photochemical synthesis of lactic acid esters. *Chem. Eng. J.* **2022**, *430*, 132550. [CrossRef]
42. Wang, S.; Pu, J.; Wu, J.; Liu, H.; Xu, H.; Li, X.; Wang, H. SO_4^{2-}/ZrO_2 as a solid acid for the esterification of palmitic acid with methanol: Effects of the calcination time and recycle method. *ACS Omega* **2020**, *5*, 30139–30147. [CrossRef]
43. Shihab, I.A.; Muhammed, M.Y.; Alheety, M.A.; Nuaman, H.A.; Karadag, A. Rapid ultrasound-assisted synthesis, characterization, DFT, molecular docking, and anticancer activity of palladium and zinc complexes with 2, 6-dimethoxybenzoic acid: A comprehensive study. *J. Mol. Struct.* **2023**, *1294*, 136259. [CrossRef]
44. Nivetha, N.; Thangamani, A.; Velmathi, S. Sulfated titania (TiO_2-SO_4^{2-}) as an efficient catalyst for organic synthesis: Overarching review from 2000 to 2021. *ChemistrySelect* **2022**, *7*, e202104505. [CrossRef]
45. Arslan-Alaton, I.; Koba-Ucun, O.; Turkten, N.; Sora, I.N.; Bekbolet, M. More about Persulfate-Assisted Ferrilanthanide-Mediated Photocatalysis of Textile Industry Dye Reactive Black 5: Surface Properties and Structural Assessment. *Water* **2023**, *15*, 906. [CrossRef]
46. Li, C.F.; Zhao, J.W.; Xie, L.j.; Wu, J.Q.; Li, G.R. Water adsorption and dissociation promoted by Co*-/NC*-biactive sites of metallic Co/N-doped carbon hybrids for efficient hydrogen evolution. *Appl. Catal. B Environ.* **2021**, *282*, 119463. [CrossRef]
47. Vargas-Villanueva, S.; Torres-Ceron, D.A.; Amaya-Roncancio, S.; Arellano-Ramírez, I.; Riva, J.S.; Restrepo-Parra, E. Study of the incorporation of S in TiO2/SO42− Coatings produced by PEO process through XPS and DFT. *Appl. Surf. Sci.* **2022**, *599*, 153811. [CrossRef]
48. Wong, W.Y.; Lim, S.; Pang, Y.L.; Chen, W.H.; Lam, M.K.; Tan, I.S. Synthesis of glycerol-free fatty acid methyl ester using interesterification reaction based on solid acid carbon catalyst derived from low-cost biomass wastes. *Int. J. Energy Res.* **2022**, *46*, 147–162. [CrossRef]
49. Mufrodi, Z.; Astuti, E.; Syamsiro, M.; Sutiman; Purwono, S. Triacetin synthesis as bio-additive from glycerol using homogeneous and heterogeneous catalysts. *Key Eng. Mater.* **2020**, *849*, 90–95. [CrossRef]
50. Banerjee, M.; Panjikar, P.C.; Bhutia, Z.T.; Bhosle, A.A.; Chatterjee, A. Micellar nanoreactors for organic transformations with a focus on "dehydration" reactions in water: A decade update. *Tetrahedron* **2021**, *88*, 132142. [CrossRef]
51. Ding, L.; Li, M.; Zhao, Y.; Zhang, H.; Shang, J.; Zhong, J.; Sheng, H.; Chen, C.; Zhao, J. The vital role of surface Brönsted acid/base sites for the photocatalytic formation of free ·OH radicals. *Appl. Catal. B Environ.* **2020**, *266*, 118634. [CrossRef]
52. Qiu, X.; Xie, X.; Meesapyodsuk, D. Molecular mechanisms for biosynthesis and assembly of nutritionally important very long chain polyunsaturated fatty acids in microorganisms. *Prog. Lipid Res.* **2020**, *79*, 101047. [CrossRef]
53. Combescot, M.; Amand, T.; Shiau, S.Y. Ab initio quantum approach to electron hole exchange for semiconductors hosting Wannier excitons. *Phys. Rev. B* **2023**, *107*, 115206. [CrossRef]
54. Wang, S.; Liu, G.; Cheng, W. Comparative evaluation of four free radical scavengers for the inhibition of individual glycidyl ester formation in rice bran oil determined by UPLC-MS/MS. *Int. J. Food Sci. Technol.* **2021**, *56*, 2983–2991. [CrossRef]
55. Ferreira, G.F.; Pessoa, J.G.B.; Pinto, L.F.R.; Maciel Filho, R.; Fregolente, L.V. Mono-and diglyceride production from microalgae: Challenges and prospects of high-value emulsifiers. *Trends Food Sci. Technol.* **2021**, *118*, 589–600. [CrossRef]
56. Chen, L.; Wang, L.; Wan, Y.; Zhang, Y.; Qi, Z.; Wu, X.; Xu, H. Acetylene and diacetylene functionalized covalent triazine frameworks as metal-free photocatalysts for hydrogen peroxide production: A new two-electron water oxidation pathway. *Adv. Mater.* **2020**, *32*, 1904433. [CrossRef] [PubMed]